Monte Carlo evaluation of spatial multiple-bit upset sensitivity to oblique incidence*

Geng Chao(耿 超)[a)b)], Liu Jie(刘 杰)[a)†], Xi Kai(习 凯)[a)b)], Zhang Zhan-Gang(张战刚)[a)b)], Gu Song(古 松)[a)b)], Hou Ming-Dong(侯明东)[a)], Sun You-Mei(孙友梅)[a)], Duan Jing-Lai(段敬来)[a)], Yao Hui-Jun(姚会军)[a)], and Mo Dan(莫 丹)[a)]

[a)] *Institute of Modern Physics, Chinese Academy of Sciences, Lanzhou* 730000, *China*
[b)] *University of Chinese Academy of Sciences, Beijing* 100190, *China*

(Received 29 November 2012; revised manuscript received 21 December 2012)

We investigate the impact of heavy ion irradiation on a hypothetical static random access memory (SRAM) device. Influences of the irradiation angle, critical charge, drain–drain spacing, and dimension of device structure on the device sensitivity have been studied. These prediction and simulated results are interpreted with MUFPSA, a Monte Carlo code based on Geant4. The results show that the orientation of ion beams and device with different critical charge exert indispensable effects on multiple-bit upsets (MBUs), and that with the decrease in spacing distance between adjacent cells or the dimension of the cells, the device is more susceptible to single event effect, especially to MBUs at oblique incidence.

Keywords: Geant4, multiple-bit upset (MBU), critical charge, spacing between adjacent cells

PACS: 95.75.–z, 61.82.Fk, 24.10.Lx **DOI:** 10.1088/1674-1056/22/5/059501

1. Introduction

The effect of spatial mutiple-bit upsets (MBUs)[1–10] has increasingly become a crucial single-event effect (SEE) problem for technology downscaling. When an incident ion is traversing the device, it is possible to generate MBUs, which give rise to the corruption of two or more physically adjacent cells, especially with the decrease in the size of electronic devices,[3,4] and the critical charge.[4] One noticeable observation from recent stuides[3–8] is that the ability of a single strike of incident particles flipping multiple-bit cells is extensively dependent on the technological device layout. Naseer *et al.*[9] presented that discrepancy in the critical charge characterization results in different estimations of soft error rates. The effect of spacing between memory cells on the MBU probablity has further been explored previously.[10] In addition, the sensitive volumes (SVs) with respect to ion track structure have been examined as a complementary aspect to analyze the MBU sensitivity. For instance, Palau *et al.*[11] discussed static random access memories (SRAMs) in response to internal ion tracks generated by nuclear reactions, and Merelle *et al.*[12] analyzed charge collection using ion tracks on a 130-nm bulk SRAM, in which the detailed characteristics of the ion track structure, particularly radial distribution of electron–hole density, have been obtained to predict MBU probabilty and multiplicity. Therefore, a realistic ion track structure appears to be more applicable, particularly in SEE characterization.

The aim of this work is to elucidate the MBU susceptibility in the case of the heavy ion irradiation at oblique incidence. We propose an analytical tool named multi-functional package of SEE analysis (MUFPSA), which has outstanding advantages of flexibly modeling various geometries of the target device, as well as incorporating underlying physical mechanisms (e.g., model of charge diffusion–collection, ion track structure profile). To be more specific, the charge collection process is modeled at diverse incident directions, and the spatial effect on MBUs is discussed. Additionally, the approach to recording the position of each cell in error allows us to distinguish patterns of spatial MBUs.

2. Principle of MUFPSA package

The package of MUFPSA based on Geant4 is a computing tool for Monte Carlo evaluation of SEEs. The Geant4 is a complete simulation toolkit for emulating the passage of particles through matter, written in C++.[13] In this work, the developed MUFPSA has the ability of deriving the radial ionization profile and spatial MBU sensitivity for specific hypothetical devices.

Previous work showed that the physical processes for SEE characterization should be composed of ionization, elastic and inelastic nuclear reaction, and multiple scattering.[14] Due to the complicated physical processes between incident ions and devices, it is more accurate to inject a space science physics list, including bosons, leptons, hadrons, neutrons, ions, and decay, into simulated physical processes. MUFPSA has indeed combined the device test structure and all the physical processes together. Besides, it develops a diffusion–collection model to detect MBUs above two bits when heavy

*Project supported by the National Natural Science Foundation of China (Grant Nos. 11179003, 10975164, 10805062, and 11005134).
†Corresponding author. E-mail: j.liu@impcas.ac.cn
© 2013 Chinese Physical Society and IOP Publishing Ltd

ions irradiate the surface of device. A detailed description of constructing device test structure and the model of charge diffusion–collection are presented as follows.

2.1. Device test structure

The hypothetical SRAM device is commonly assumed to be composed of two superposed layers, as shown in Fig. 1(a). The overlayers are made of SiO_2 as the first layer, and the substrate corresponding to the second layer is made of natural silicon. The layer of the SVs is where the charge collection happens. In addition, it is frequently associated with the depletion region, for the charges generated in the depletion region are collected very efficiently within the SV via the drift process. Therefore, when energetic ions pass through a microelectronic device, the SVs are reponsible for charge creation and collection, which makes it a crucial and prerequisite ingredient in predicting the SEU occurrence.

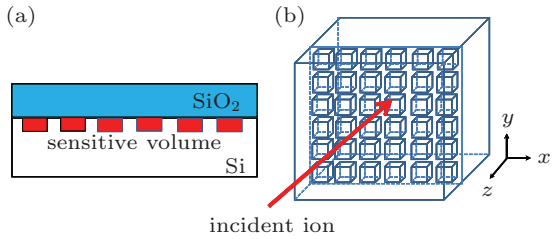


Fig. 1. (color online) Structural chart of 6×6-bits SRAM cell architecture for device simulation. (a) Front view of a hypothetical device. Interconnect and passivation layers have been simulated with a cuboidal surface area. (b) Three-dimensional diagram of the process of incident ions traversing through the device outputted by MUFPSA.

The relative locations of incident ions and the device under irradiation are illustrated in Fig. 1(b). In reality, if incident ions travel through the air layer before interacting with the device, the incident energy will be attenuated. Thus, it is supposed that ions strike directly upon the device surface. In addition, to achieve the validity and accuracy of heavy ion testing, all the incident beams are performed as mono-energetic and randomly striking the surface of device. As can be seen in Fig. 1, a pattern of 6×6-bits SRAM cells is defined and replicated as the actual layout. The main reason for this design and architecture is that the device SEU sensitivity to incident ions depends on whether the deposited energy within the SVs exceeds the critical energy or not. Consequently, this test structure allows us to identify accurately the multiplicity and spatial distribution of MBUs.

2.2. A model for charge diffusion–collection

It has been revealed that charge sharing between drains has an impact on the amount of charges collected by drains, and accordingly, on the MBU sensitivity. Therefore, to study spatial MBU sensitivity, several adjacent cells mentioned above were modeled in a three-dimensional (3D) domain.

For the convenience of checking mappings of incident ion impacts, the SVs have been labelled with numbers. Detailed arrangement and the parameter of spacing are illustrated in Fig. 2(a). The merit of the MUFPSA package is that charge generation and collection have been taken into consideration not only for those happening within the irradiated SVs, but also for the charge diffused in the neighboring SVs, as depicted in Fig. 2(b). Moreover, omnidirectional charge collection has been simulated by combining energy deposition and electron–hole pairs' collection along the track over 2π steradians. The radial distribution of charge density is optimized to be suitable for heavy ions in silicon materials, and given by

$$D(r) = \frac{2.84\times10^4 Z^{*2}}{3.6\alpha\beta^2 t(t+T)}\left(\frac{R-t}{R+T}\right)^{1/\alpha}(1+K(t)),$$
$$K(t) = A\left(\frac{t-B}{C}\right)\mathrm{e}^{-((t-B)/C)}, \quad (1)$$

where $D(r)$ is the charge density in a coaxial cylindrical shell of thickness dt at a distance t from the path of an incident ion of effective Z^* moving with a relative velocity $\beta = v/c$ through silicon. In addition, $K(t)$ is the corrected expression, $B = 0.1$ nm, and A and C are the parameters about β.

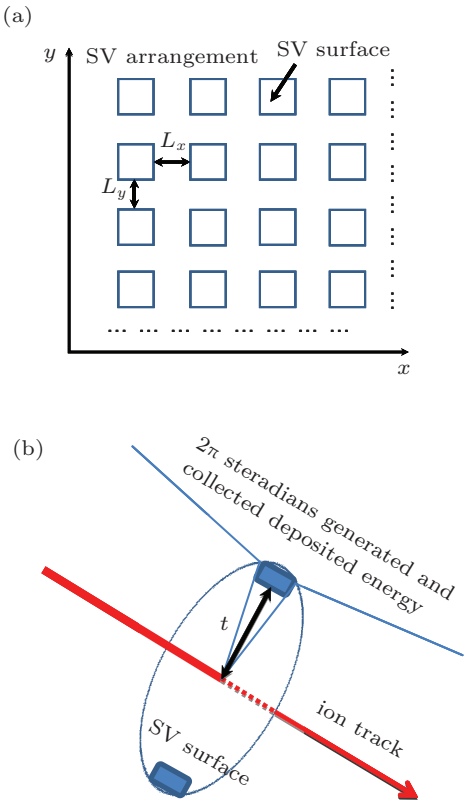


Fig. 2. (color online) (a) Top view of SVs. Here, L_x and L_y are the drain-to-drain spacing along the x and y axis. (b) Schematic cross section of the process of generating and collecting charge when an incident ion strikes the device. The parameter t denotes the radial distance from the ion path.

Ultimately, in the integration of the marked SV arrangement and omnidirectional charge collection, the model of charge diffusion–collection reveals the influence of radial ionization profile on SEU occurrence, especially on the MBU sensitivity.

3. Validation of MUFPSA through the simulated results

To identify SEEs in virtual radiation environment, the classical curve of SEU cross section versus the linear energy transfer (LET) is an effective and accurate criterion for testing the ability of MUFPSA. In the section, SEE studies have been typically performed in a mono-energetic heavy ion irradiation environment. As for the species of commonly-accelerated incident ions in heavy ion research facility in Lanzhou (HIRFL) SEE experiment, heavy ion irradiation parameters of ion species, energy, and range in silicon, listed in Table 1, have been input into MUFPSA.

Table 1. Heavy ion irradiation parameters in silicon used during Monte Carlo evaluation of SEEs.

Ion	Energy/MeV	Effective LET /MeV·cm^2·mg^{-1}	Range/μm
^{40}Ar	268.41	12.03	77.42
	146.24	15.45	38.54
^{132}Xe	10887.97	18.48	1600
	8012.80	22.63	991.54
	4656.33	32.00	444.18
	2521.00	45.05	197.74
	1112.57	61.82	81.49
^{209}Bi	6369.43	65.00	350.62
	4305.13	75.06	223.05

According to the device test structure, it is supposed that the number of incident ions on the device is N, and the cuboidal surface is S_{origin}. An SEU occurrence at the i-th incident ion is denoted by n_i. Thus, SEU cross section can be given by

$$\sigma = P(S_{\text{origin}}, S_{\text{real}}) \frac{S_{\text{origin}}}{N} \sum_{i=i(Q_{\text{crit}})}^{\infty} n_i, \tag{2}$$

where $P(S_{\text{origin}}, S_{\text{real}}) = S_{\text{origin}}/S_{\text{real}}$, S_{origin} is a constant for a specific testing device, and S_{real} is the real area of the device striked by ions. In addition, the i-th incident ion is assumed to go through the device and create charge Q_i. If $Q_i \geq Q_{\text{crit}}$ ($i = 1, 2, \ldots, n$), one bit flip happens. For SEU calculation,

$$n_i = \begin{cases} 0, & (Q_i < Q_{\text{crit}}), \\ 1, & (Q_i \geq Q_{\text{crit}}). \end{cases} \tag{3}$$

The MUFPSA has been performed for heavy ion irradiation in combination with the above-mentioned principles. In this section, the irradiated device has been simulated as 90-nm SRAMs in accordance with Ref. [15]. The length and width of the SV are identical and defined as L, and spacing $L_x = L_y$. During the simulated irradiation, for each heavy ion source, each simulation run consists of 10^4 primary incident ions (using the general particle source) striking perpendicularly (along the Z axis) on the device test structure (see Fig. 1).

As shown in Fig. 3, the SEU cross sections have been evaluated as a function of LET. The cell-to-cell spacing ranges from 0 to L in simulations. It is clear that the SEU cross sections decrease linearly when the spacing increases, which apparently results from the fact that closer adjacent SVs make incident ions traverse SVs with larger probability. In spite of the influence of the drain-to-drain spacing on the sensitivity to SEU cross section, it should be noted that no MBU event was detected for spacing close to the cell dimensions.

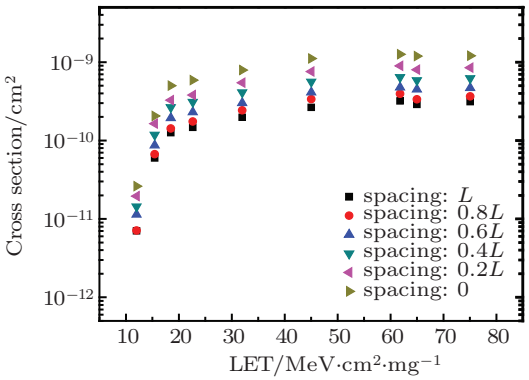


Fig. 3. (color online) Sensitivity curve of the SEU cross section versus the LET.

Currently, the results of the heavy ion irradiation for SEE characterization are most conveniently described by a Weibull fitting, which is also a function of the LET in the form of

$$\sigma = \sigma_{\text{sat}} \left\{ 1 - \exp\left[-\left(\frac{L - L_{\text{th}}}{W} \right)^S \right] \right\}, \tag{4}$$

where σ_{sat} is the saturation value or the limiting and plateau cross section, L_{th} is the LET threshold value, W and S are fitting parameters, W denotes the width, and S is a dimensionless exponent.

It is a practical and simple method of calculating the theoretical upset cross section versus LET curve and verifying the Weibull fitting function. On the basis of the curves of cross section as functions of the LET, it is revealed that simulated results are in very good agreement with the Weibull fitting function. In addition, the Weibull parameters for all spacing SEU cross sections are listed in Table 2.

4. Influence factors in SEU/MBU sensitivity

As the integration of SRAM continuously increases, while its characteristics gradually decreases, the problems of SEE become increasingly serious, particularly under the effect of MBU. Therefore, the impact of radial ionization

Table 2. Fitting parameters of the Weibull function from the evaluation of SEEs.

Spacing	L_{th}/MeV·cm^2·mg^{-1}	W/MeV·cm^2·mg^{-1}	S	σ_{sat}/cm^2	R^2
0	11.65	17.15	1.00	1.26×10^{-9}	0.98
0.2L	11.49	19.18	0.98	8.98×10^{-10}	0.98
0.4L	11.74	16.70	0.93	6.41×10^{-10}	0.98
0.6L	11.62	16.85	0.97	4.76×10^{-10}	0.98
0.8L	11.81	18.68	0.93	3.92×10^{-10}	0.97
1.0L	11.87	22.62	0.81	3.50×10^{-10}	0.98

profile on the SEU occurrence becomes significant, especially in the case that a particle generates a radial distribution of electron–hole pairs of nearly the same order of size as that of an elementary transistor. In Ref. [16], ion track structures were studied, and an analytical model was proposed for ions in arbitrary materials. In particular, previous studies have demonstrated that radial ionization profile plays a vital role in explaining the effect of the ion mass and energy on the response of the device.[4,9] In this section, another novel approach is performed to simulate the radial ionization profile of the irradiated beam.

The spatial distribution of energy deposition density from incident ions and secondary particles has been evaluated as a function of the radial distance from deposits to the ion path. The results are plotted in Fig. 4, which are well consistent with the previous work.[4,9] In addition, given that the maximum range of δ rays is $R_{max} = 67827$ nm, the track radius of incident ion 30.48 MeV/u ^{209}Bi is indeed larger than the deep-submicron device's SVs. Moreover, if the size of the SV is smaller than the track radius, part of heavy ion charge will not participate in the process of charge collection. Consequently, we conclude that the excursion outside of the ion track may induce variations in charge collection and have an impact on the device response to the SEU/MBU sensitivity.

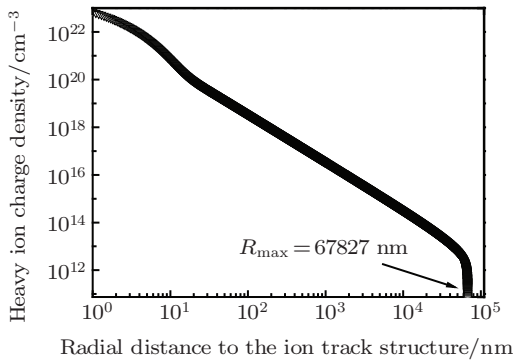


Fig. 4. Distribution of the heavy ion charge/electron–hole density of incident ions ^{209}Bi (30.48 MeV/u) in silicon along the radial direction.

Followed by the description of radial ionization profile of incident ions, the simulation approach combining Geant4 and MUFPSA is then applied to study the factors that influence SEU/MBU sensitivity and the dependence of SEU/MBU sensitivity on oblique incident effects (using 30.48-MeV/u incident ion ^{209}Bi) with critical charge and the spacing in adjacent cells.

4.1. Oblique incident effects

As in the diffusion–collection model, when an incident ion travels through a device at an oblique angle, it can probably disturb the neighboring SV, as shown in Fig. 5.

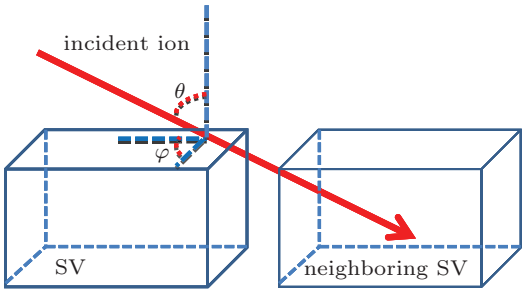


Fig. 5. (color online) Schematic diagram of the ion track structure affecting the neighboring SV in an oblique incidence way.

In order to take the contribution of incident ions at the oblique angle to the amount of charge into consideration, the way in which incident ions traverse on the surface area of device also invokes the program of general particle source. The detailed angular distribution is given by

$$P_x = -\sin\theta\cos\varphi, \quad P_y = -\sin\theta\sin\varphi, \quad P_z = -\cos\theta. \quad (5)$$

In all the simulations, the MBU rate is calculated by

$$R_{MBU} = \frac{N_{MBU}}{N_{SEU}} \times 100\%, \quad (6)$$

where N_{MBU} is the number of incident ions arousing more than one error, and N_{SEU} is the number of incident ions causing at least one error.

4.1.1. MBU multiplicity with different angles

Our simulated results indicate that angled strikes have a significant effect on SVs, and hence affect MBU multiplicity. Theoretically, the total number of patterns of SEUs probably induced by incident ions is given by

$$N_{pattern} = \sum_{k=0}^{n} C_n^k, \quad (7)$$

where k is the number of flipped bit cells, and n is the number of bit cells. For a specific device, n is a constant. In this work, $n = 36$.

As expected, the presence of many MBUs, even more than 5 cells, has been observed in the process of angled strikes. For instance, patterns of spatial MBUs, such as SBU, DBU, and TBU, are presented in Fig. 6. These mappings verify the feasibility and accuracy of MUFPSA in modeling the MBU probability and multiplicity.

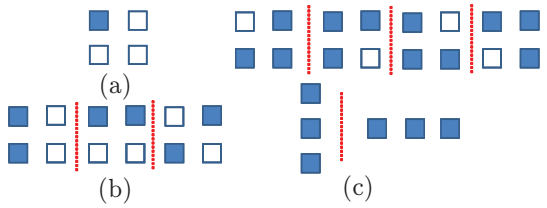


Fig. 6. (color online) Examples of patterns of spatial MBUs in an SEU. (a) Single-bit upset; (b) double-bit upset; (c) triple-bit upset. Open box: normal bit cell; solid box: flipped bit cell.

4.1.2. MBU sensitivity with critical charge

In an attempt to predict accurately the MBU sensitivity in the condition of an oblique incident effect, we keep the 90-nm SRAM geometry but change the critical charge to observe the distinction of MBU probability and multiplicity.

The results are depicted in Fig. 7. The ratio of heavy-ion MBU is a function of incident angle with three different critical charges: 0.8, 4.0, and 20 fC. As can be seen in Fig. 7, although MBU probability has some discrepancy at 20° and 80° incident angle, the difference of MBU probability at 40° and 60° is larger for different critical charges. An explanation lies in the differences in charge collection. In the cases of 20° and 80° incidence angle, the collected charges are distributed in an extreme condition, compared with critical charge, most of which are located around the critical charge. However, in middle-angled cases, collected charges are mainly distributed at a larger fluctuation relative to critical charge. Moreover, the induced errors are easier to be observed and their patterns become diverse when increasing the incident angle. Especially, at higher angle of 80°, 6-bit upsets have been detected at lower critical charge of 0.8 and 4.0 fC, whereas no 6-bit upsets have been found at 20 fC.

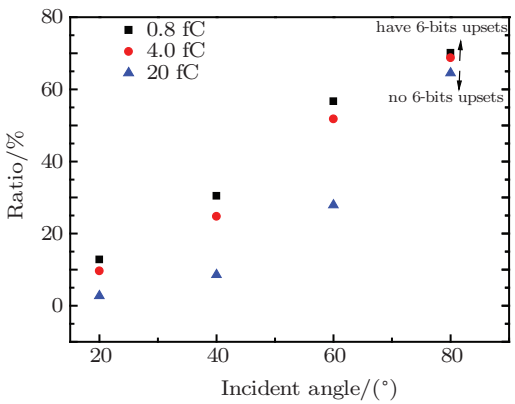


Fig. 7. (color online) Ratio of heavy-ion MBU between numbers of MBUs and SEUs as a function of incident angle for three different values of spacing.

The detailed partition of SBU and MBU along with the variables of incident angle and critical charge are shown in Fig. 8. These simulations make it clear that MBU multiplicity gradually increases as critical charge decreases and incident angle increases. Especially in the case of incident angle 80°, MBU (≥ 3) has been observed. For instance, in the worst environment of critical charge 0.4 fC and angle 80°, SBU is only 29.91% of the total bit failure, whereas MBU (≥ 3) is 18.35%. Thus, with incident angle increasing, MBU becomes more diverse and its multiplicity gets larger with decreasing critical charge.

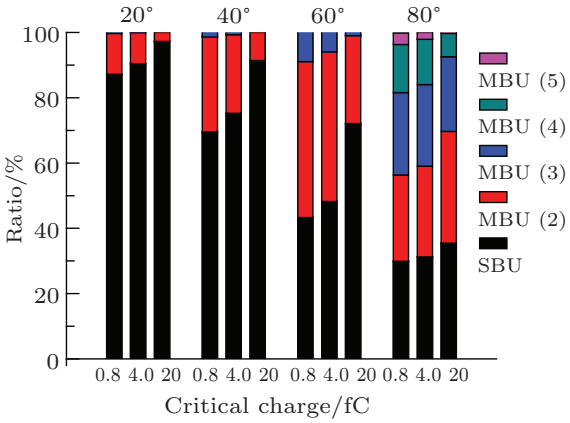


Fig. 8. (color online) Ratio of single-bit upset and multiple-bit upset.

4.2. Spacing between adjacent cells

The spacing between adjacent cells plays a vital role in the calculation of MBU multiplicity. Previous studies demonstrated that closer sensitive nodes in adjacent cells would give rise to more MBU multiplicity.[15,17] Besides, the MBU rates were proved to decrease exponentially when the spacing increases.[17] Therefore, it is quite important to quantify the effect of spacing between adjacent cells on MBU sensitivity.

The heavy-ion MBU probability as a function of incident angle for four different values of spacing are shown in Fig. 9. The cell-to-cell spacing ranges from 0 to L in simulations. This indicates that, the layout topology greatly affects the ratio of the heavy ion MBU. As shown in Fig. 9, MBU probabilities

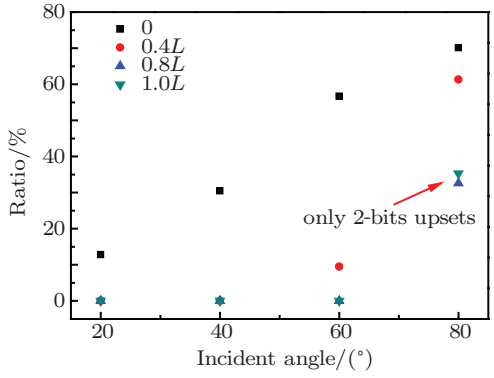


Fig. 9. (color online) Ratio of heavy-ion MBU to SEU as a function of incident angle for four different values of spacing.

for different spacings (0, 0.4L, 0.8L, L) are drastically different no matter what the incident angle is. The MBU probability increases with increasing angle because of the diffused track structure model mentioned above, in which the influence of radial distribution of δ rays is taken into account. When spacing is smaller, the effect of δ rays or radial ionization profile on MBU sensitivity would be greater. Thus, spacings of 0 and 0.4L lead to larger MBU multiplicity at an incident angle of 80°, whereas only 2-bit upsets have been obtained under the conditions of 0.8L and L.

In addition, the specific MBU multiplicity and percentage of SBU and MBU are presented in Fig. 10. It shows the proportion of SBU and MBU versus incident angle and spacing. As revealed by the worst part of incident 80°, the MBU multiplicity decreases as the spacing increases. However, MBU multiplicity at the incident angle 80° is still larger than that at other angles. With regard to spacing at incident angle 80°, MBU ($\geq$ 2) comprising 70.09% and MBU ($\geq$ 5) have been observed at spacing of 0, whereas only MBU (2) has been obtained at spacing of 0.8L and L. These simulations display adequately that MBU multiplicity resulting from the diffusion model is affected not only by incident angle, but also by spacing.

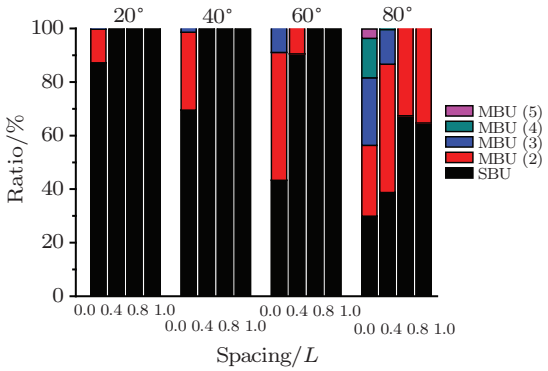


Fig. 10. (color online) Proportion of single-bit upset and multiple-bit upset.

4.3. Dimensions of the simulated device

Concerning device scaling, the main parameters for the SEU and MBU susceptibilities are discussed in aspect of layout properties. In this section, heavy-ion irradiations are carried out on 65-nm and 45-nm SRAMs respectively to investigate the effect of the cell area on MBU sensitivity. The characteristics of the studied SRAMs in this work are illustrated in Table 3. The critical charge and silicon film thickness are referred to in previous work.[3,18]

Table 3. Characteristics of the studied SRAMs for layout properties.

Technological node/nm	Cuboidal surface area/μm^2	SV surface/μm^2	Silicon film thickness/nm	Critical charge/fC
65	0.625	0.132×0.132	60	0.6
45	0.400	0.105×0.105	50	0.5

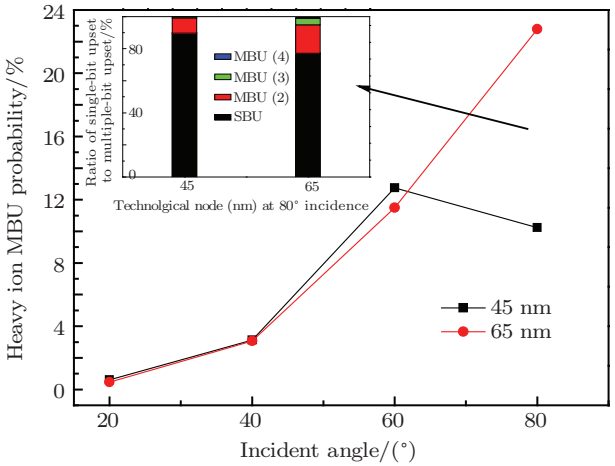


Fig. 11. (color online) Evaluation of MBU probability at 30.48 MeV/u Bi ion irradiation with different incident angles. Inset: contribution of event multiplicity in total event SEUs for the extreme angular incidence.

With the integration of parameters in Table 3 and MUFPSA evaluation, the results of heavy-ion MBU probabilities are obtained on the condition of 30.48 MeV/u Bi traversed (see Fig. 11). The inset shows the event multiplicity in total event SEUs at the extreme angular incidence.

As shown in Fig. 11, increasing trends of MBU probability and multiplicity have been observed when increasing incident angle until 60°. The 45-nm device presents more MBU and higher multiplicity than the 65-nm technology does, which has a decent agreement with previous literatures.[3,5] It is however interesting that the 65-nm technological mode has higher MBU probability than the 45-nm mode does. The emerged exceptional data point in the 45-nm technological device at 80° incidence is probably derived from the improper ratio of the dimensions of cuboidal surface area and the thickness of layers to the size of SVs. Consequently, the over-layer SiO_2 is deleted to clarify the emerged odd situation at 80° incidence as a complementary study.

Figure 12 exposes clearly that MBU probability increases slightly from 45 to 65 nm technology, and the abnormal data point has virtually disappeared. The trends for MBU probability as incident angle increases are reasonable and similar to the previous work.[3] Similarly, the higher-multiplicity events appear at incident angle 80°, as the inset shows. The 45-nm technological mode has higher multiplicity than 65-nm one does:

MBU ($\geq$ 2) 68.73% and MBU (5) 0.69% for the former, and MBU ($\geq$ 2) 66.61% and MBU (5) 0.21% for the latter, respectively. Thus, the influence of over layer can dominate the MBU sensitivity, including MBU probability and multiplicity. Therefore, it is recommended that studies on device layout and dimensions should first characterize the over-layer effects and radial ionization profile.

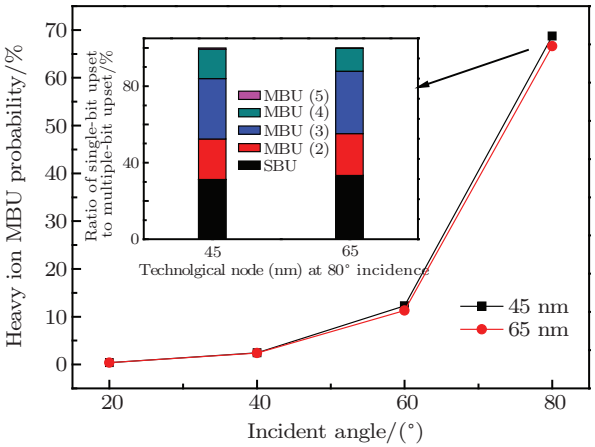


Fig. 12. (color online) Heavy-ion MBU probability as a function of incident angle on the architecture without over layers by a 30.48 MeV/u Bi ion. Inset: contribution of event multiplicity in total event SEUs for the extreme angular incidence.

5. Discussion

This work is performed for some hypothetical devices. In view of different critical charges and spacing between adjacent cells, our results seem to be applicable to other devices for heavy-ion irradiation, through varying the parameters of device geometry and incident beams. However, it should be recognized that this work focuses mainly on the physical process, while overlooks the electrical property of device. It is possible that some other simulated results would be different for the characterization of MBU sensitivity if considering electrical field inside device.

In addition, as to the particular section of dimensions of device analysis, the unusual phenomenon attracted our great attention to the radial distribution of energy deposition. Therefore, if we ignore the over-layer effects on the energy deposition, simulating accumulated energy will be meaningful for the interpretation of MBU probability and multiplicity.

As mentioned above, to study the role of radial track structure more deeply, we offered an explanation based on the simple diffusion–collection mechanism which states that charges are accumulated within the area of radius along the radial direction of an incident ion. In Fig. 13, the observation of accumulated charge is induced by 30.48 MeV/u ^{209}Bi in silicon at the depth of 80 nm. The accumulated charge decreases with the area's growth. In addition, it is important to point out that the maximum accumulated charge is 32.3 fC at the first area of radius 0.5L, which is several times larger than the critical charge. Therefore, it is reasonable that these incident ions have the ability of triggering MBUs. Furthermore, from the radial ionization point, it is equally demonstrated that the interpretation of MBU characterization and susceptibility should factor spacing in adjacent cells and dimensions of devices. Consequently, utilizing a detailed radial ionization profile for MBU, predication and analysis of SRAMs become a necessity, especially at oblique incidence.

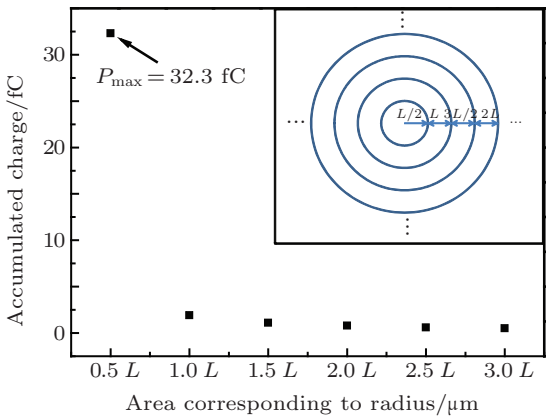


Fig. 13. (color online) Accumulated charge within the area of radius along the radial direction of incident ion 30.48 MeV/u ^{209}Bi in silicon at the depth of 80 nm.

6. Conclusion

In this work, SBU and MBU occurrence in simulated SRAMs have been investigated using MUFPSA. An advantage of MUFPSA is that it has successfully combined the diffusion–collection model and radial ionization tracks of incident ions along with device simulations. With the diffusion–collection model, it is substantially observed that an ion track penetrating the SVs might induce MBU multiplicity. After validation of the MUFPSA, the variability of the MBU probability is then simulated and discussed on oblique effects with MBU multiplicity and different critical charge, spacing in adjacent cells, and dimensions of device.

The evaluation of MBU multiplicity and the corresponding probability at oblique incidence have been done because it contributes greatly to the exploration and recognition of MBU susceptibility. Incident angle is proved to have an influence on the charge collection and radial distribution of heavy-ion charge density along with the ion track, and thus on the sensitivity of SBUs and MBUs. As a conclusion, on the relevance of the detailed impact parameters of critical charge, spacing between adjacent cells, and dimensions of the device, it is demonstrated that with the decrease in the critical charge and spacing between adjacent cells, MBU probability and multiplicity are getting larger, which can also arise from increasing incident angle. In addition, the influence of dimensions of de-

vice on MBU sensitivity is more involved in the device testing structure, especially in over layers.

References

[1] Zhang Q X, Hou M D, Liu J, Wang Z G, Jin Y F, Zhu Z Y, Sun Y M and Zhang Q X 2004 *Acta Phys. Sin.* **53** 566 (in Chinese)

[2] Zhang K Y, Guo H X, Luo Y H, He B P, Yao Z B, Zhang F Q and Wang Y M 2009 *Acta Phys. Sin.* **58** 8651 (in Chinese)

[3] Raine M, Hubert G, Gaillardin M, Paillet P and Bournel A 2011 *IEEE Trans. Nucl. Sci.* **58** 2607

[4] Giot D, Roche P, Gasiot G and Harboe-Sorensen R 2007 *IEEE Trans. Nucl. Sci.* **54** 904

[5] Raine M, Hubert G, Paillet P, Gaillardin M and Bournel A 2012 *IEEE Trans. Nucl. Sci.* **59** 950

[6] Amusan O A, Massengill L W, Baze M P, Bhuva B L, Witulski A F, DasGupta S, Sternberg A L, Fleming P R, Heath C C and Alles M L 2007 *IEEE Trans. Nucl. Sci.* **54** 2584

[7] Radaelli D, Puchner H, Skip W and Daniel S 2005 *IEEE Trans. Nucl. Sci.* **52** 2433

[8] Suh J, Annavaram M and Dubois M 2012 *The 18th International Symposium on High Performance Computer Architecture*, February 25–29, 2012 New Orleans, USA, p. 1

[9] Naseer R, Boulghassoul Y, Draper J, DasGupta S and Witulski A 2007 *International Symposium on Circuits and Systems*, May 27–30, 2007 New Orleans, USA, p. 1879

[10] Roche P, Gasiot G, Forbes K, O'Sullivan V and Ferlet V 2003 *IEEE Trans. Nucl. Sci.* **50** 2046

[11] Palau J M, Hubert G, Coulie K, Sagnes B, Calvet M C and Fourtine S 2001 *IEEE Trans. Nucl. Sci.* **48** 225

[12] Merelle T, Serre S, Saigne F, Sagnes B, Gasiot G, Roche P, Carriere T and Palau M C 2006 *IEEE Trans. Nucl. Sci.* **53** 1897

[13] Agostinelli S, Allison J, Amako K, *et al.* 2003 *Nucl. Instrum. Method Phys. Res. A* **506** 250

[14] Warren K M, Weller R A, Mendenhall M H, Reed R A, Ball D R, Howe C L, Olson B D, Alles M L, Massengill L W, Schrimpf R D, Haddad N F, Doyle S E, McMorrow D, Melinger J S and Lotshaw W T 2005 *IEEE Trans. Nucl. Sci.* **52** 2125

[15] Giot D, Roche P, Gasiot G, Autran J L and Sorensen R H 2007 *The 9th European Conference on Radiation and Its Effects on Components and Systems*, Septemper 10–14, 2007 Deauville, France, p. 1

[16] Cucinotta F A, Katz R, Wilson J W and Dubey R R 1996 *Faculty Publications* p. 62

[17] Merelle T, Saigne F, Sagnes B, Gasiot G, Roche P, Carriere T and Palau M C 2005 *The 8th European Conference on Radiation and Its Effects on Components and Systems*, September 19–23, 2005 Cap D'Agde, France, p. E3-1.

[18] Heidel D F, Marshall P W, LaBel K A, *et al.* 2008 *IEEE Trans. Nucl. Sci.* **55** 3394